RSC Advances

PAPER

View Article Online
View Journal | View Issue



Cite this: *RSC Adv.*, 2024, **14**, 33312

# An ESIPT-active orange-emissive 2-(2′-hydroxyphenyl)imidazo[1,2-*a*]pyridine-derived chemodosimeter for turn-on detection of fluoride ions *via* desilylation†

Akhil A. Bhosle, Mainak Banerjee,* Ankit Thakuri, Pooja D. Vishwakarma and Amrita Chatterjee*

Fluoride is an essential element for oral health with an optimum concentration of 0.7–1.2 ppm in drinking water, but it is detrimental at higher concentrations, causing fluorosis, acute gastric ulcer, urolithiasis, and kidney infection, which adds immense significance to its detection in water sources. In the current study, a new chemodosimeter (**HIPS-Br**) is designed by protecting a 2-(2′-hydroxyphenyl)imidazo[1,2-*a*]pyridine derivative (**HIP-Br**) with a fluoride recognizable *tert*-butyldiphenylsilane moiety and utilized for the selective detection of $F^-$ ions by an excited-state intramolecular proton transfer (ESIPT)-based fluorimetric response. The probe **HIPS-Br** exhibits blue fluorescence in solution, and upon the incremental addition of $F^-$ ions, it exhibits a turn-on response, exhibiting a strong orange emission at 598 nm by spontaneous cleavage of the *tert*-butyldiphenylsilane group to release fluorescent **HIP-Br** in the working solution. **HIPS-Br** displayed no or insignificant response towards numerous common anions, cations and small molecules, affirming its selectivity to $F^-$ ions and offered a low limit of detection (LOD) of 1.2 ppb ($6.6 \times 10^{-8}$ M). The real sample analysis by spiking fluorides in water and toothpaste samples showed excellent percent recoveries. The chemodosimeter was successfully utilized in the solid-phase detection of $F^-$ ions on silica-coated TLC plates and analyzed by ImageJ analysis, marking its utility in on-site quantitation purposes.

Received 11th August 2024
Accepted 9th October 2024

DOI: 10.1039/d4ra05823b

rsc.li/rsc-advances



## 1. Introduction

Fluoride ($F^-$) ions are essential micronutrients for proper growth and maintenance of hair, nails, bones, and teeth.[1] For its beneficial effects on human body, $F^-$ ions are used as an additive in toothpaste and drinking water.[2,3] Groundwater contains sufficient fluoride ions due to the dissolution of fluoride-rich rocks that primarily contribute to the daily intake of fluoride.[4,5] Otherwise, anthropogenic activities and the widespread use of fluoride-containing products cause high $F^-$ assimilation in soil and water.[6] The World Health Organization (WHO) recommends an optimum fluoride concentration of 0.7–1.2 ppm in water supplies through artificial fluoridation.[7] Besides their vital roles in physiological functions and biomedical applications, such as the treatment of osteoporosis,[8] high intake of fluoride ions can cause dental and skeletal fluorosis,[9,10] acute gastric and kidney infections,[11,12] urolithiasis,[13,14] and even cancer at excessive concentrations.[15,16] Because of the adverse effects of fluoride in higher concentrations, the United States Environmental Protection Agency (USEPA) has proposed a permissible limit of 4 ppm for fluoride in drinking water.[17] Considering that the detection and accurate estimation of fluoride ions is essential for human and environmental welfare, several fine analytical techniques based on sophisticated instruments, including ion chromatography,[18,19] high-performance liquid chromatography,[20,21] atomic absorption spectrometry (AAS)[22] and $^{19}F$ NMR,[23] have been developed for the detection of $F^-$ ions. Apart from these expensive tools, researchers have paid attention to developing various colorimetric and fluorimetric sensors owing to the high sensitivity, selectivity, and portability of these molecular probes.[24,25] These chemosensors depend on either the strong hydrogen bonding of $F^-$ ions or a deprotonation step driven by $F^-$ ions to generate the parent chromophore utilizing its strong affinity towards electropositive boron, silicon, antimony, *etc.*[26–30] However, many of these chemosensors/chemodosimeters involve multiple synthetic steps and solution-phase reactions and are not explored for on-site detection, making the development of cost-effective and sensitive chemodosimeters necessary.

Small molecule fluorophores with a special property of intense emission in the solid state have attracted considerable

*Department of Chemistry, Birla Institute of Technology and Science, Pilani, KK Birla Goa Campus, Goa 403726, India. E-mail: mainak@goa.bits-pilani.ac.in; amrita@goa.bits-pilani.ac.in; Fax: +91-832-255-7031; Tel: +91-832-2580-347; +91-832-2580-320*

† Electronic supplementary information (ESI) available. See DOI: https://doi.org/10.1039/d4ra05823b

research attention in sensing and bioimaging with a focus on on-site device applications.[31] This is in contrast to conventional organic dyes, which suffer from the aggregation-caused-quenching (ACQ) effect in concentrated solutions or in the solid state.[32] Many a time, the enhanced emission is caused by the restriction in the intramolecular rotation around the single bond in conjugated aromatic systems (a class of compounds called AIEgens)[33,34] or intramolecular flipping of H-atom between two hetero-atoms (such as N- and O-) at the excited state, a phenomenon known as excited-state intramolecular proton transfer (ESIPT).[35–37] To date, the most commonly studied ESIPT-active compounds are 2-(2′ hydroxyphenyl)benzothiazole (**HBT**),[38,39] 2-(2′-hydroxyphenyl)benzimidazole (**HBI**),[40,41] 2-(2′-hydroxyphenyl)benzoxazole (**HBO**),[42,43] and their analogues.

Imidazo[1,2-*a*]pyridine, an important class of heterocycle[44,45] shows immense biological activities and is quite ubiquitous among several pharmaceutical products.[46,47] In addition, it possesses inherent fluorescence properties and, lately, has been employed in chemosensing applications by tuning its photophysical properties by appropriate structural modifications.[48,49] Imidazo[1,2-*a*]pyridines with a 2′-hydroxyphenyl unit at C-2 is another class of ESIPT-active compound; however, there are only limited studies on their photophysical properties[50,51] and chemosensing applications.[52,53] The vast synthetic modality for this scaffold is advantageous for photophysical tunability, leading to large Stokes shifts needed for chemosensing applications. With our growing interest in the use of ESIPT-active luminogens for chemosensing applications,[36,38,54] we paid our attention to developing 2-(2′-hydroxyphenyl)imidazo[1,2-*a*] pyridine-derived chemodosimeter for the selective and sensitive detection of fluoride ions exploiting its affinity towards silicon-atom. Keeping the perspective of current environmental concerns, a sustainable and organic solvent-free mechanochemical method[55,56] was adopted for the synthesis of the probe, **HIPS-Br**.

# 2. Experimental section

## 2.1 Chemicals and reagents

5-Bromo-2-hydroxyacetophenone, 2-aminopyridine and *tert*-butylchlorodiphenyl silane of AR grade were purchased from TCI India Pvt. Ltd. Other common chemicals, salts, and common solvents of LR grade were obtained from various other commercial suppliers and used without further purification. To monitor the progress of the reaction, thin-layer chromatography (TLC) was used on silica gel plates (0.25 mm, 60F-254). The TLC was visualized using UV lamps with wavelengths of 254 nm and 365 nm. For real sample analysis, water samples were collected from different local water bodies and different brands of toothpaste were procured and utilized as such from the local market. Ultrapure deionized water was obtained from a Millipore water system (18 MΩ cm) and was purged with $N_2$ for 15 minutes before use.

## 2.2 Instrumentation and measurements

The mechanochemical reactions were conducted with a RETSCH MM400 instrument, utilizing a 5 mL grinding jar and a 10 mm ball of stainless steel (SS). A 500 MHz Bruker Avance NMR spectrometer was used to record the NMR spectra. LCMS and HRMS spectra were acquired from Agilent LC-MS (model 6460 Triple Quadrupole LC/MS) and HRMS (model 6545 QTOF), respectively, using an ESI ion source. JASCO V770 and FP-8500 model UV-vis spectrophotometer and spectrofluorimeter were used with the data pitch and bandwidth fixed at 1 nm and excitation and emission slit widths maintained at 2.5 nm for all the UV-vis and fluorescence experiments, respectively. Ion chromatography was done on Metroohm Eco IC with 944 professional UV/vis detector, Vario. The photographs for solid-phase studies were captured using a 64-megapixel smartphone (Oneplus 11R) and subjected to ImageJ software for analysis.

## 2.3 Synthesis of the probe, HIPS-Br

The probe, **HIPS-Br**, was synthesized by adopting a two-step mechanochemical route.

(a) Synthesis of 4-bromo-2-(imidazo[1,2-*a*]pyridin-2-yl) phenol (HIP–Br):[57] 5-Bromo-2-hydroxyacetophenone (**1**) (112 mg, 0.5 mmol), 2-aminopyridine (**2**) (61 mg, 0.65 mmol) and iodine (38 mg, 0.15 mmol) were taken in a 5 mL stainless steel (SS) milling jar containing a 10 mm SS ball. The mixture was milled using silica gel (500 mg, 60–120 mesh) as the solid matrix in an MM400 instrument at 25 Hz for 2 h. The slurry was subjected to flash chromatography and eluted with EtOAc–petroleum ether (1 : 4) to afford pure **HIP-Br** as a yellowish-orange solid (123 mg, yield: 82%); $^1$H NMR (500 MHz, $CDCl_3$): $\delta$ (ppm) 12.77 (s, 1H), 8.16 (d, $J$ = 6.7 Hz, 1H), 7.85 (s, 1H), 7.69 (d, $J$ = 2.5 Hz, 1H), 7.59 (d, $J$ = 9.0 Hz, 1H), 7.30–7.24 (m, 2H), 6.92–6.87 (m, 2H); $^{13}$C {$^1$H} NMR (125 MHz, $CDCl_3$): $\delta$ (ppm) 156.4, 143.9, 143.6, 132.2, 128.1, 125.6, 125.5, 119.5, 118.0, 116.9, 113.4, 110.7, 107.0.

(b) Synthesis of 2-(5-bromo-2-((tert-butyldiphenylsilyl)oxy) phenyl)imidazo[1,2-*a*]pyridine (**HIPS-Br**): In a 5 mL SS milling jar, **HIP-Br** (72 mg, 0.25 mmol), *tert*-butylchlorodiphenylsilane (**3**) (75 mg, 0.27 mmol) and imidazole (88 mg, 1.25 mmol) were mixed with silica gel (350 mg, 60–120 mesh) and milled in an MM400 at 25 Hz for 3 h. The slurry of the crude product was subjected to flash chromatography to get the final probe **HIPS-Br** as a yellow solid (115 mg, yield: 88%); $^1$H NMR (500 MHz, $CDCl_3$): $\delta$ (ppm) 8.45 (d, $J$ = 2.6 Hz, 1H), 8.33 (s, 1H), 8.02 (d, $J$ = 6.7 Hz, 1H), 7.65 (d, $J$ = 9.0 Hz, 1H), 7.47–7.36 (m, 11H), 7.18 (t, $J$ = 7.9 Hz, 1H), 6.94 (dd, $J_1$ = 8.7 Hz, $J_2$ = 2.6 Hz, 1H), 6.77 (t, $J$ = 7.9 Hz, 1H), 1.14 (s, 9H); $^{13}$C {$^1$H} NMR (125 MHz, $CDCl_3$): $\delta$ (ppm) 151.7, 144.5, 140.3, 136.3, 134.8, 132.1, 131.9, 130.6, 130.2, 129.5, 128.0, 127.6, 126.2, 125.4, 124.8, 121.5, 117.4, 114.1, 113.0, 112.4, 26.9, 19.4; HRMS (ESI-TOF): $m/z$ calcd for $C_{29}H_{27}N_2OBrSi$ $[M + H]^+$ 527.1149, found 527.1151.

## 2.4 Analytical procedures

In order to perform spectrofluorimetric analyses, a stock solution of 1 mM **HIPS-Br** in THF was prepared. A 1 mM stock solution of fluoride ($F^-$) was prepared from its tetrabutylammonium salt in deionized water (Milli-Q, 18 MΩ cm). Deionized water was used for dilution purposes as per the

requirement of the spectrofluorimetric studies. For the selectivity studies, stock solutions of different anions were prepared from the corresponding sodium or potassium salts, and nitrates or chlorides were used for the solutions of different cations. Organic small molecules were dissolved either in THF or water as per their solubility. Different toothpaste samples were vacuum-dried and the fine powder was dissolved in water (1 g in 20 mL water) by sonicating for 30 min and incubated for 24 h. A part of the supernatant was collected, diluted with water and used for real sample analysis in toothpaste. Any particulate matter in the solutions was discarded by filtering through 0.22 μm syringe filters before each analysis. After excitation at 350 nm, all of the fluorimetric data were acquired between 355 and 750 nm. The spectroscopic analyses were carried out at room temperature (25 °C), and the average data for each analysis is based on three repetitions.

### 2.5 Calculation of fluorescence quantum yield

Fluorescence quantum yield was calculated using the equation:

$$\varphi_x = \varphi_{std} \times \frac{I_x}{I_{std}} \times \frac{A_{std}}{A_x} \times \frac{{n_x}^2}{{n_{std}}^2}$$

where $\varphi$ = quantum yield, $I$ = emission intensity, $n$ = refractive index, and $A$ = optical density, std = standard quinine sulphate, and x = **HIP-Br**.

### 2.6 Calculation of the limit of detection

The limit of detection was calculated from the $3\sigma/k$ equation where $\sigma$ = standard deviation and $k$ = slope of the linear regression equation.

### 2.7 DFT calculations

The density functional theory (DFT)[58] was used to carry out theoretical studies, and for the time-dependent density functional theory (TD-DFT)[59–61] level, the Gaussian 09 program was used.[62] Becke's three-parameter exchange function (B3) with the Lee-Yang-Parr correlation (LYP) function was employed using a 6-31G basis set for the optimization of molecular geometries.

### 2.8 Solid-phase sensing of $F^-$ using HIPS-Br

For solid-phase sensing of $F^-$ ions, silica gel-coated TLC plates were taken and cut into small strips and dipped in the probe solution in $CH_2Cl_2$ (100 μM) for a few seconds and air-dried. Further, $F^-$ (1, 2, 5, 10, 15, 20, 25, 30, 40 and 50 ppm) concentrations prepared in water were drop-casted on **HIPS-Br**-coated TLC strips. TLC strips were allowed to be air dried at room temperature, further incubated for 1 h, then visualized under a 365 nm UV lamp.

## 3. Results and discussion

### 3.1 Design and synthesis of the probe, HIPS-Br

From our earlier studies on the mechanochemical synthetic protocols for imidazo[1,2-*a*]pyridines,[63,64] we observed that 2-(2′-hydroxyphenyl)imidazo[1,2-*a*]pyridines emit solvent-dependent strong fluorescence by ESIPT, quite similar to 2-hydroxyphenylbenzothiazoles (**HBT**), with a higher Stokes shift. Considering a heavy atom like –Br would help a bathochromic shift of $\lambda_{max}$, we planned to synthesize the chemodosimiter (**HIPS-Br**) from the para-bromo derivative of 2-(2′-hydroxyphenyl)imidazo[1,2-*a*]pyridine (**HIP-Br**). Considering fluoride can perform spontaneous desilylation, the probe, **HIP-Br**, was planned to be protected by the *tert*-butyldiphenylsilane group. In a two-step sustainable approach, **HIPS-Br** was synthesized by mechanochemical mixer-milling of 2-hydroxy-5-bromoacetophenone and 2-aminopyridine in the presence of iodine as the catalyst and silica as the grinding matrix to afford **HIP-Br** in 82% isolated yield. Subsequently, the phenolic –OH group of **HIP-Br** was protected in a mechanochemical manner by mixing *tert*-butylchlorodiphenylsilane and imidazole with silica as the grinding matrix and milling at 25 Hz for 3 h affording the chemodosimeter, 2-(5-bromo-2-((*tert*-butyldiphenylsilyl)oxy)phenyl)imidazo[1,2-*a*]pyridine (**HIPS-Br**), in an excellent yield (Scheme 1). **HIPS-Br** was characterized using $^1$H NMR, $^{13}$C NMR, and HRMS analyses. The disappearance of the peak at $\delta$ 12.77 corresponding to the phenolic –OH and the presence of a singlet at $\delta$ 1.41 corresponding to the *tert*-butyl unit in $^1$H NMR indicated the formation of the probe, **HIPS-Br**. Similarly, the presence of peaks at $\delta$ 26.9 and 19.4 corresponding to the quaternary carbon and the methyl groups of the *tert*-butyldiphenylsilane moiety in $^{13}$C NMR confirmed the formation of the chemodosimeter, **HIPS-Br**.

### 3.2 Photophysical properties of HIP-Br

The imidazopyridine scaffold was anticipated to emit strong fluorescence with higher Stokes shifts in the orange-to-red region due to its intramolecular proton transfer properties similar to **HBT**. Consequently, the solubility and photophysical properties of the probe, **HIP-Br**, were initially assessed in various organic solvents. As expected, **HIP-Br** was highly soluble and exhibited solvent-dependent emission in diverse polar protic and polar aprotic solvents, including DCM, ACN, THF, DMF, DMSO, MeOH, and EtOH. The UV-visible absorption spectrum of **HIP-Br** (30 μM) in THF revealed a strong absorption band at 350 nm with an additional shoulder peak at 362 nm (Fig. S1, ESI†). Subsequently, the emission properties of **HIP-Br**

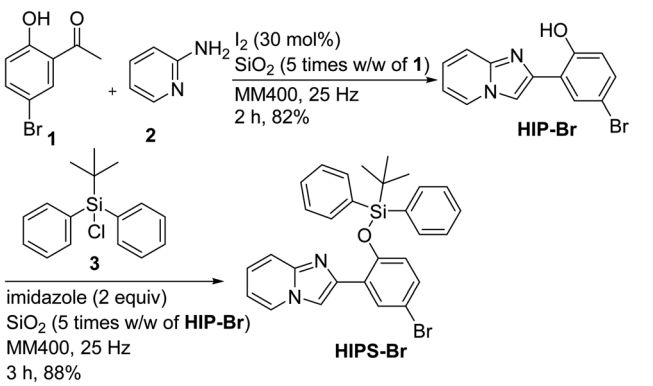


Scheme 1 Synthesis of the HIPS-Br probe.

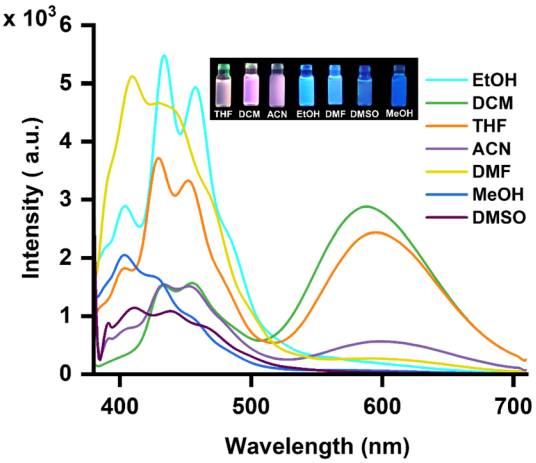


Fig. 1 Fluorimetric responses of HIP-Br (10 μM) in different organic solvents depicting intense orange emission in THF and DCM and relatively lower emissions in other polar protic and polar aprotic solvents ($\lambda_{ex}$ = 350 nm, $\lambda_{em}$ = 598 nm) [inset: images of HIP-Br under UV light in different solvents].

(10 μM) were examined with an excitation wavelength of 350 nm. It was noticed that **HIP-Br** displayed two intense emissions at around $\lambda_{max}$ 430 nm and 598 nm in DCM and THF. However, when switching to a polar protic solvent such as EtOH, a notable decrease in emission intensity of the peak at 598 nm was observed while the peak at 430 nm retained its intensity (Fig. 1). Therefore, the proton transfer between oxygen and nitrogen atoms *via* ESIPT is facile in a polar aprotic solvent allowing the orange emission channel on. Whereas, in polar protic solvent, presumably, the solvation of the phenolic-OH functionality causes hindrance in the proton transfer process; thereby, only inherent blue emission of imidazopyridine was observed from **HIP-Br** (Fig. 1, inset). The probe displayed a quantum yield of 5.74% and 5.72% in THF and DCM at $\lambda_{max}$ 598 nm with a relatively high Stokes shift taking quinine sulfate as standard,[65] whereas, in DMF and EtOH, a higher quantum yield of 9.10 and 9.72 at $\lambda_{max}$ 430 nm was observed (Table 1). The possible aggregation-induced emission (AIE) behavior of **HIP-Br** was evaluated by gradually increasing the water fractions in water–THF mixtures. However, the probe demonstrated a progressive decrease in emission intensity at 598 nm, with negligible fluorescence in 50% water–THF fractions or above, indicating the absence of typical AIE characteristics (Fig. S2, ESI†). The loss of emission at the red-shifted peak is an indication of diminished ESIPT behavior due to the solvation effect by water around the phenolic-OH group. Notably, the fluorescence loss is nominal at 10% $H_2O$–THF, giving scope for the detection of water-soluble analytes by the probe. Since 2-(2′hydroxyphenyl)benzothiazole (**HBT**) is an important class of ESIPT active fluorophores, the photophysical properties of **HIP-Br** were compared with that of **HBT-Br**. Interestingly, **HIP-Br** displayed a larger Stokes shift of 250 nm in THF and a higher quantum yield than its congener **HBT-Br** (190 nm, 1.25%, Table S1, ESI†), generating our interest for further photophysical studies on this scaffold, tuning its electronic properties by the introduction of suitable substituents; however, these studies are not a part of this article. Similar to **HIP-Br**, **HIPS-Br** showed a UV-vis band at around 350 nm and fluoresced blue at $\lambda_{max}$ 409 nm when excited at 350 nm (Fig. S3, ESI†). However, the orange emission peak was absent for **HIPS-Br** as there is no scope for ESIPT. The emission characteristics of **HIP-Br** were analyzed over a broad pH range (pH 3–12). The fluorescence of **HIP-Br** was unperturbed at the near-neutral pH (pH 6–8), with the most intense emission occurring at physiological pH 7, offering its potential for sensing applications under physiological conditions (Fig. S4, ESI†). Notably, **HIPS-Br** also withstood a pH change from pH 6–12 but gradually disintegrated in strongly acidic solutions (Fig. S4, ESI†). It gives us the working range for using **HIPS-Br** as the chemodosimeter. The chemodosimeter **HIPS-Br** was examined in various THF–water fractions, but it displayed no fluorescence across all water fractions, likely due to the inhibition of the excited state intramolecular proton transfer phenomenon (Fig. S5, ESI†). Although **HIP-Br** displayed significant emission in both THF and DCM, considering the prevalence of fluoride ions in water, all studies were carried out in THF-water mixtures (9 : 1). Before proceeding further, a time-dependent response study with **HIPS-Br** (10 μM) and fluoride ions (60 μM) was conducted, which showed that the maximum fluorescence output was achieved within just 2 min (Fig. S6, ESI†).

### 3.3 DFT studies

DFT studies were carried out to align the theoretical predictions with the optical properties of the probe **HIPS-Br** and **HIP-Br** as per experimental observations. The optimized structure of

Table 1 Photophysical properties of HIP-Br in different solvents

| | | Absorbance (nm) | | Emission (nm) | | | | | Quantum yield ($\varphi$) (%) | |
|---|---|---|---|---|---|---|---|---|---|---|
| S. no | Solvent | $\lambda_{abs1}$ | $\lambda_{abs2}$ | $\lambda_{em1}$ | Int. | $\lambda_{em2}$ | Int. | Stokes shift (nm) | $\varphi_1$ | $\varphi_2$ |
| 1 | DCM | 250 | 351 | 455 | 1567 | 590 | 2873 | 239 | 7.82 | 5.72 |
| 2 | THF | 246 | 348 | 454 | 3324 | 598 | 2435 | 250 | 3.11 | 5.74 |
| 3 | ACN | 251 | 351 | 456 | 1505 | 601 | 559 | 250 | 2.00 | 0.71 |
| 4 | DMF | — | 351 | 411 | 4432 | — | — | 60 | 9.10 | — |
| 5 | DMSO | — | 351 | 441 | 2549 | — | — | 90 | 5.32 | — |
| 6 | EtOH | 263 | 349 | 459 | 4498 | — | — | 110 | 9.72 | — |
| 7 | MeOH | 243 | 349 | 428 | 2906 | — | — | 79 | 3.22 | — |

**HIPS-Br** in the excited state revealed a significant electron population spread across the entire molecular framework, with greater density on the imidazopyridine ring. **HIP-Br** also displayed a similar electron population but with greater electron delocalization in the oxygen atom. The molecular structure obtained after intramolecular proton transfer **HIP-Br$_{IPT}$**, in contrast, displayed a higher electron population on the phenolic ring. The calculated band gaps between the LUMO and HOMO of **HIPS-Br** (−0.15724) and **HIP-Br** (−0.15715) were reasonably low, allowing decent electronic population at the excited states upon absorbing light, and upon falling back to $S_0$, it results in the inherent blue fluorescence from the imidazo [1,2-*a*]pyridine framework. After a proton transfer, the band gap of **HIP-Br$_{IPT}$** was found to be significantly low (−0.06683) by DFT calculations, which is indicative of a facile ESIPT process and responsible for orange emission upon excitation of **HIP-Br** at 350 nm (Fig. 2). The LUMO–HOMO orbital transition mainly contributes (98%) to the $S_1$–$S_0$ emission transition with an oscillator strength of 0.1716. Additionally, the proton transfer could lead to the distribution of the positive charge between the N-atoms, resulting in a structure with greater charge separation.[51]

### 3.4 Fluoride ion sensing studies using HIPS-Br

In order to ensure the sensitive detection of fluoride ions, the fluorimetric responses of **HIPS-Br** (10 μM in 10% water–THF) solution were recorded at 598 nm upon the incremental addition of $F^-$ ions. Upon the addition of $F^-$ ions to **HIPS-Br**, a gradual increase in emission intensities at 598 nm was noticed, while the fluorescence band at 410 nm was mostly unaffected (Fig. S7, ESI†). The increase was proportional to $F^-$ ion concentrations, and the saturation point was obtained upon the addition of 60 μM of $F^-$ with a 12-fold increase in the fluorescence output (Fig. 3a). A high regression coefficient of 0.9966 was obtained upon plotting the graph of the ratios of relative intensities of the probe at 598 nm as a function of $F^-$ concentration (Fig. 3b). In a complementary analysis, we focused on the detection of $F^-$ ions at lower concentration ranges and observed a strong linear correlation within the 0–10 μM range, with a high regression coefficient ($R^2$ = 0.9947). Using this data, the limit of detection (LOD) was calculated as $6.6 \times 10^{-8}$ M (1.2 ppb) using the equation $3\sigma/k$, where $\sigma$ is the standard deviation and $k$ is the slope (Fig. 3c). As **HIPS-Br** displays a strong absorption band in the UV-vis spectrum, a study monitoring the absorption changes in the presence and absence of $F^-$ ions was performed. The study revealed just a slight shift of 10 nm in the spectrum of **HIPS-Br** upon adding $F^-$ ions without any other noticeable changes (Fig. S8, ESI†).

### 3.5 Selectivity of HIPS-Br towards $F^-$

After successfully demonstrating the sensitive detection of fluoride ions ($F^-$), the subsequent critical step was to evaluate and address potential interferences from other analytes in the sensing process. A thorough investigation was conducted to identify possible competitors to $F^-$, encompassing various anions, metal ions, and neutral molecules. To assess their impact, these analytes were introduced in substantial excess (300 μM) to a 10 μM solution of **HIPS-Br**, and their individual responses were meticulously recorded. Encouragingly, no significant increase in fluorescence intensity at 598 nm was

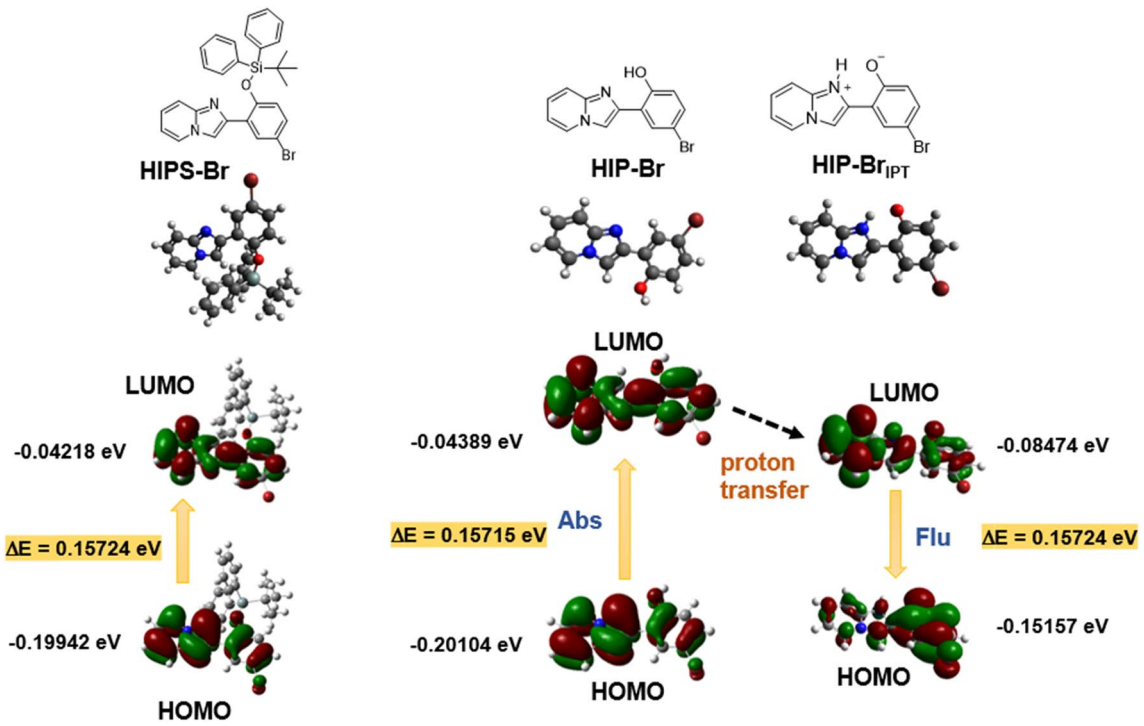


Fig. 2 Optimized structures, visualized electron distribution and energy levels of LUMO and HOMO of HIPS-Br, HIP-Br and HIP-Br$_{IPT}$.

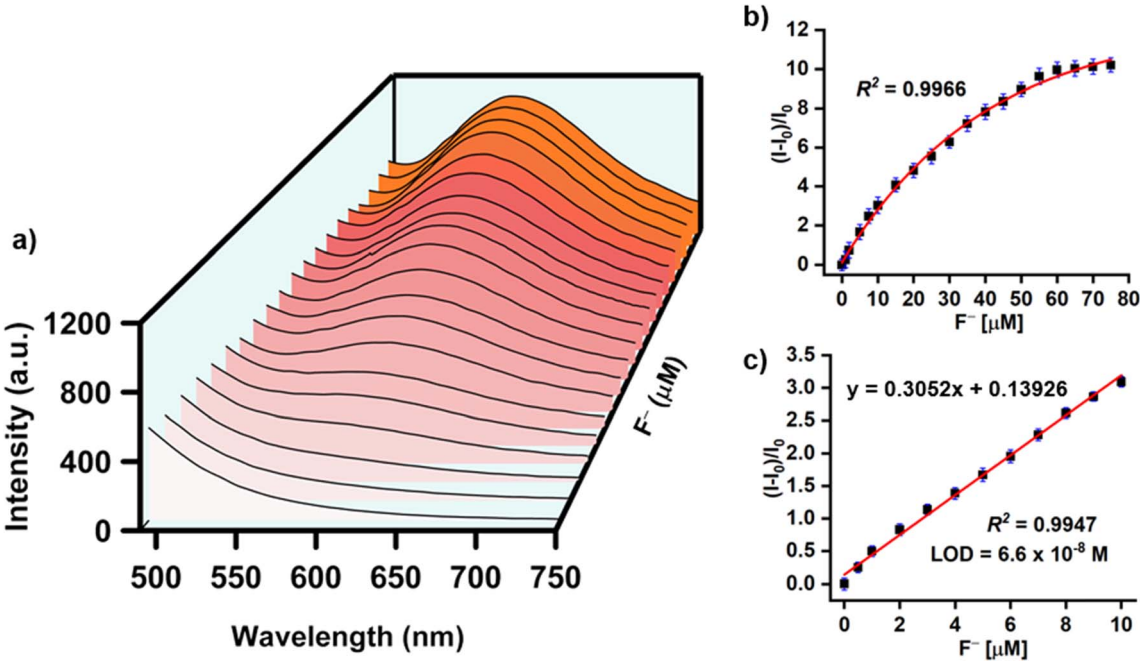


Fig. 3 (a) Fluorescence spectral output of **HIPS-Br** (10 μM in 10% water–THF) upon gradual addition of $F^-$ (0–80 μM) ($\lambda_{ex}$ = 350 nm; $\lambda_{em}$ = 598 nm). (b) Plot of the ratio of fluorescence intensities against $F^-$ concentrations (0–80 μM). (c) Fluorimetric responses of **HIPS-Br** (10 μM) at lower concentrations of $F^-$ (0–10 μM) ($\lambda_{ex}$ = 350 nm, $\lambda_{em}$ = 598 nm).

observed upon the addition of anions like $Cl^-$, $Br^-$, $I^-$, *etc.*, metal ions such as $Na^+$, $Mg^{2+}$, $Al^{3+}$, *etc.*, and neutral molecules like urea, HMTA, dopamine, *etc.* (Fig. 4). These consistent outcomes in all the studies confirmed the selectivity of the probe **HIPS-Br** towards $F^-$. The chemodosimetric approach, which leverages the highly specific fluoride-mediated cleavage of the *O*-silyl bond, facilitates the selective detection of fluoride ions.

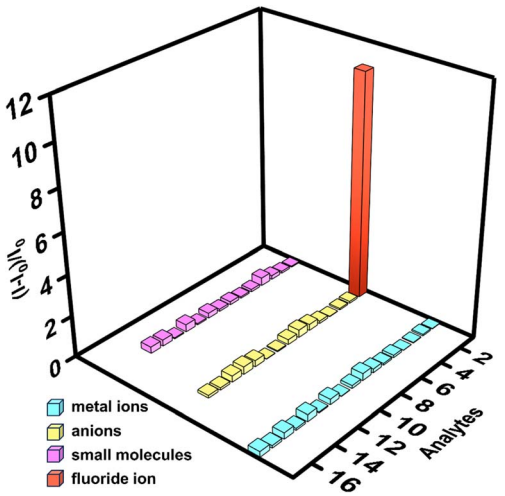


Fig. 4 Fluorimetric responses of various metal ions ((1) $Na^+$, (2) $Mg^{2+}$, (3) $Al^{3+}$, (4) $K^+$, (5) $Ca^{2+}$, (6) $Cr^{3+}$, (7) $Mn^{2+}$, (8) $Fe^{2+}$, (9) $Fe^{3+}$, (10) $Co^{2+}$, (11) $Ni^{2+}$, (12) $Cu^{2+}$, (13) $Zn^{2+}$, (14) $Pd^{2+}$, (15) $Ag^+$, (16) $Hg^{2+}$, (17) $Pb^{2+}$), anions (1) $F^-$, (2) $Cl^-$, (3) $Br^-$, (4) $I^-$, (5) $CN^-$, (6) $N_3^-$, (7) $HS^-$, (8) $HO^-$, (9) $NO_3^-$, (10) $NO_2^-$, (11) $SO_4^{2-}$, (12) $PO_4^{3-}$, (13) $SCN^-$, (14) $ClO^-$, (15) $S^{2-}$), neutral molecules ((1) urea, (2) HMTA, (3) dopamine, (4) $Et_3N$, (5) guanine, (6) benzylamine, (7) $Et_2NH$, (8) 2-aminopyridine, (9) 3-aminopyridine, (10) dicyclohexylamine, (11) pyridine, (12) melamine, (13) 4-aminopyridine, (14) dodecylamine) (300 μM) towards **HIPS-Br** (10 μM) under optimized conditions ($\lambda_{ex}$ = 350 nm; $\lambda_{em}$ = 598 nm).

### 3.6 Sensing mechanism

The sensing mechanism relies on the strong affinity between silicon and fluoride ions. **HIPS-Br** was protected by a bulky silyl functionality. Fluoride, because of its ability to form a strong Si–F bond, serves as the most efficient deprotection agent, resulting in a spontaneous and fast cleavage of the Si–O bond at room temperature. The desilylation of **HIPS-Br** resulted in the formation of **HIP-Br** in solution, restoring the orange emission by ESIPT (Scheme 2). Presumably, the formation of the charged intermediate at the excited state *via* proton transfer is responsible for the larger Stokes shift as compared to its HBT derivative (Scheme 2a). To further confirm the sensing mechanism, an LCMS analysis of **HIPS-Br** was carried out before and after the addition of fluoride. Before $F^-$ ion addition, the spectrum displayed two peaks of equal intensity centered at *m*/*z* 527, 529 corresponding to **HIPS-Br** $[M + H]^+$. After the addition of fluoride, peaks at *m*/*z* 289 and 291, corresponding to **HIP-Br** $[M + H]^+$, were observed with a bromide pattern in MS retained (Scheme 2b). These observations confirmed the proposed chemodosimetric behavior of **HIPS-Br**. The electron distribution obtained through TD-DFT studies indicates that in **HIPS-Br**, greater electron density resides on the imidazopyridine ring, giving it blue fluorescence, whereas in the ESIPT-active state (**HIP-Br$_{IPT}$**), greater delocalization is seen on the phenolic ring, giving rise to its orange emission.

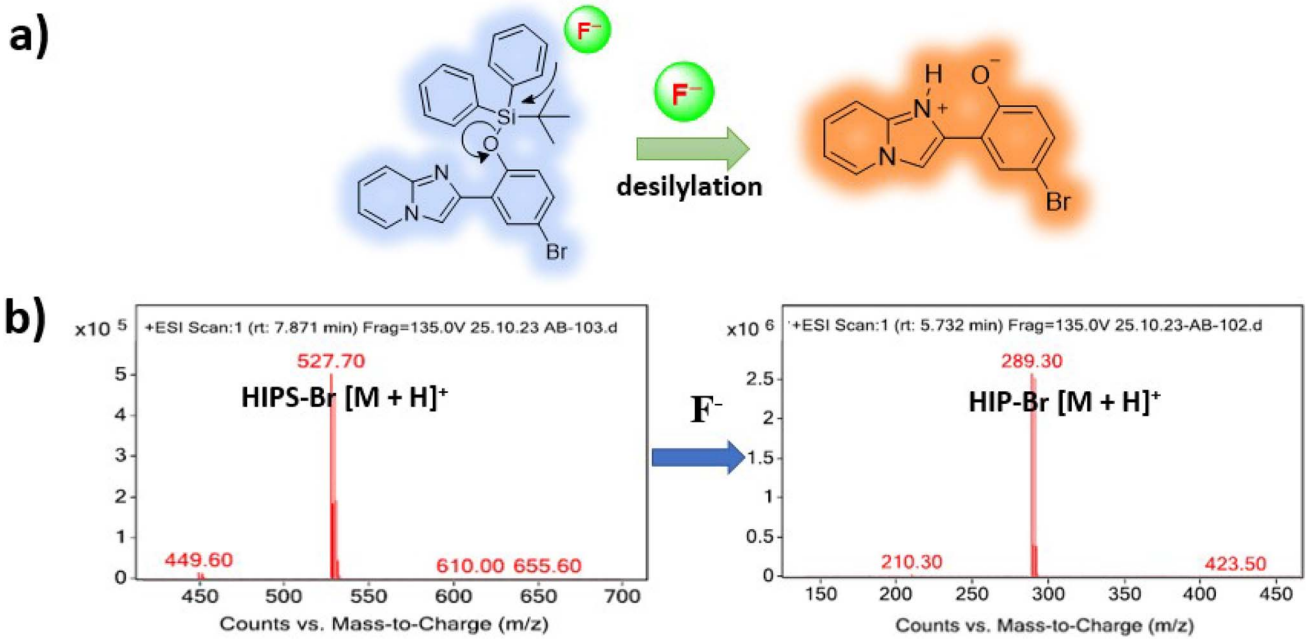


Scheme 2 (a) Schematic of the sensing mechanism of fluoride ions with the probe, HIPS-Br. (b) The mass spectra of the probe before and after treatment of fluoride ions.

### 3.7 Determination of $F^-$ in real samples using HIPS-Br

To demonstrate the practical applicability of the imidazopyridine-based sensing system in real-world scenarios, water samples were collected from various sources, including ponds, rivers, seas, taps, lakes, and rain, and were subsequently spiked with predetermined concentrations of fluoride ions ($F^-$). These spiked samples were treated with the probe **HIPS-Br** sensing assay, and their fluorescence output was recorded. All measurements were performed in triplicate, yielding a relative standard deviation (RSD) within 3–4%, which signifies the reproducibility of the data. The percent recovery for all real samples was above 100%, indicating the efficient performance of the sensing assay in detecting fluoride ions in real water samples (Table 2). The higher recovery also suggests the natural presence of fluoride ions in real water samples. To further validate, we tested the probe's performance on several toothpaste brands, all of which had a maximum fluoride content of 1000 ppm. The extraction process involved drying the toothpaste, then sonicating 1 g of the dried mass in 20 mL of water for 30 min and further incubation for 24 h. After centrifugation, the aqueous supernatant was used for real sample analysis of fluoride in toothpaste samples. After initial calibration with known fluoride concentrations, fluoride sample extracts from different concentrations of toothpaste were analysed by fluorimetric analysis, and the corresponding concentrations were obtained from the standard plots and presented in ppm. These results of fluoride contents in the toothpaste samples were compared with ion chromatography (IC) data for further validation (Table 3). The values from the developed probe closely matched those from IC, confirming the high accuracy of the newly developed probe for fluoride estimation in real samples.

### 3.8 Solid phase detection of $F^-$ ions

Recently, smartphone-based devices have been effectively employed in the detection and quantification of analytes through rapid image analysis, emerging as a user-friendly approach for on-site detection.[38] To our advantage, the small molecule probe, **HIP-Br**, is strongly fluorescent in the solid phase due to the restriction of molecular motion at the ESIPT-

Table 2 The %recovery of real sample analysis in different food samples pre-spiked with a known concentration of $F^-$ ions

| S. no | Sample | $F^-$ added (μM) | $F^-$ found (μM) | Recovery (%) | RSD ($n = 3$) |
|---|---|---|---|---|---|
| 1 | Tap water | 1.5 | 1.53 | 102.0 | 2.8 |
| 2 | River water | 3.5 | 3.61 | 103.1 | 3.2 |
| 3 | Field water | 5.5 | 5.76 | 104.7 | 2.6 |
| 4 | Pond water | 7.5 | 7.92 | 105.6 | 3.1 |
| 5 | Lake water | 9.5 | 9.90 | 104.2 | 3.5 |

Table 3 Real sample analysis data for different toothpaste samples. Comparison between IC and HIPS-Br for fluoride detection

| Toothpaste | Conc. from IC (ppm) | Conc. from probe **HIPS-Br** (ppm) |
|---|---|---|
| 1 | 0.946 | 0.95 |
| 2 | 0.764 | 0.72 |
| 3 | 0.882 | 0.9 |
| 4 | 0.765 | 0.74 |
| 5 | 0.685 | 0.72 |

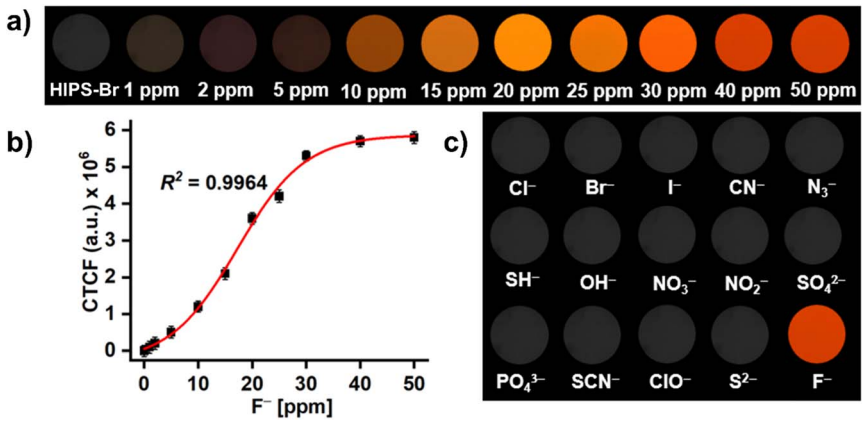


Fig. 5 (a) Fluorescence photographs of silica-coated TLC strips soaked in **HIPS-Br** solution (100 μM) and drop-casted with different concentrations of $F^-$ (0–50 ppm), photographed under 365 nm UV light. (b) The corresponding CTCF plots. (c) Solid-phase fluorimetric responses of **HIPS-Br** coated TLC strips after the addition of 50 ppm of various competing analytes.

active state (**HIP-Br$_{IPT}$**) by the transfer of H-atom from phenolic –OH to ring nitrogen. For the purpose of solid-phase detection, we prepared strips of **HIPS-Br** using silica-coated TLC plates as the solid platform. The TLC strips were prepared by dipping them into the probe solution (100 μM in DCM) and subsequent air drying. **HIPS-Br** did not display its inherent fluorescence in the solid phase (on TLC strips), presumably due to aggregation-caused quenching (ACQ). The dried strips were then dipped into an aqueous solution with varying concentrations of fluoride ions. All strips dipped into the fluoride solutions displayed bright orange fluorescence proportional to the concentration of fluoride (Fig. 5). The images of the strips were taken through a mobile camera (One plus 11R, 64 MP) and analyzed through ImageJ software to generate the count of total fluorescence (CTCF) values. For the analysis of each sample, four different regions within the circular area were randomly selected using the background as a control. The CTC values of the images were plotted against the concentrations of fluoride ions. Notably, the solid phase provided a significant fluorescence response in the 0–50 ppm fluoride range, with a regression coefficient of $R^2 = 0.9964$ (Fig. 4). The sensor was able to detect 1 ppm of fluoride in the solid state, displaying enhanced fluorescence. Notably, the USEPA set a limit for fluoride in drinking water as 4 ppm, which is well above the lower detection limit of the current protocol in the solid phase. This demonstrates the potential of using image analysis techniques for the quantification of fluoride in real-life applications. A selectivity study with several common anions was also conducted in the solid phase to ensure the specificity of **HIPS-Br**-coated TLC strips towards fluoride ions. Only fluoride ions displayed a significant response in the strips, displaying the selective nature of the chemodosimeter.

### 3.9 Comparative study

Finally, a comparative assessment of the imidazopyridine-based sensor (**HIPS-Br**) with other available methods, focusing on sensitivity, selectivity, and applicability, was conducted using selected ESIPT-based and desilylation strategy-based molecular probes for fluorimetric detection of fluoride ions. As shown in Table S2 of ESI,† the current probe has a lower detection limit, fast signal transduction compared to other molecular probes in consideration, and is synthesized by a green and solvent-free approach, mechanosynthesis, which is a sheer advantage over others. The two-step high-yielding synthesis makes this molecular probe more cost-effective than others. Additionally, the use of **HIPS-Br**-coated TLC strips demonstrates better ability in solid-phase estimation of fluoride in real samples, enabling the scope of on-site real-world applications.

## 4. Conclusion

In this study, we developed an efficient ESIPT-active orange-emissive chemodosimeter, **HIPS-Br**, for the selective and sensitive turn-on detection of fluoride ions ($F^-$). The probe was synthesized using a sustainable mechanochemical approach, which is both cost-effective and environmentally friendly. **HIPS-Br** demonstrated remarkable selectivity towards $F^-$ ions over a range of common anions, cations, and small organic molecules. The probe's strong orange emission at 598 nm upon interaction with $F^-$ ions provides a significant advantage for fluorimetric detection over other blue-emissive ESIPT probes, ensuring high sensitivity and accuracy. The sensing mechanism relies on the strong affinity of Si and fluoride ions, which leads to the desilylation of **HIPS-Br** to generate orange emissive **HIP-Br** with an impressive detection limit of 1.2 ppb, which is significantly lower than the USEPA limit for fluoride in drinking water (4 ppm). Furthermore, the solid-phase detection capability on silica-coated TLC plates marks the probe's utility for on-site and real-time fluoride quantitation, enhancing its practicality for diverse applications. The sensor was able to detect fluoride levels as low as 1 ppm in the solid phase. The successful application of **HIPS-Br** in real sample analysis, including spiked water, with excellent recovery rates, underscores its potential for practical applications in environmental monitoring and public health. This work not only presents a highly sensitive chemodosimeter for fluoride detection but

also opens new avenues for developing sustainable and efficient sensing materials for various analytes. Our findings highlight the importance of integrating green chemistry principles in sensor design, paving the way for future advancements in analytical chemistry and environmental sciences.

## Data availability

This is to declare that the data of this work will be available on request from readers for the following manuscript titled "An ESIPT-active orange-emissive 2-(2′-hydroxyphenyl)imidazo[1,2-*a*]pyridine-derived chemodosimeter for turn-on detection of fluoride ions *via* desilylation".

## Author contributions

A. A. B.: investigation, analysis, validation. M. B.: conceptualization, supervision, resources, writing – original draft, review & editing. A. T.: validation, visualization, writing – review & editing. P. D. V.: investigation, validation. A. C.: supervision, resources, writing – review & editing.

## Conflicts of interest

The authors declare no personal, financial, or organizational conflict of interest.

## Acknowledgements

A. A. B. expresses gratitude to BITS Pilani, KK Birla Goa Campus, for the research fellowship. A. T. is thankful to BITS Pilani, KK Birla Goa Campus, for the research fellowship. NMR and LCMS data were obtained from the Central Sophisticated Instrumentation Facility (CSIF), BITS Pilani, KK Birla Goa Campus.

## References

1 C. M. Carey, Focus on Fluorides: Update on the use of fluoride for the prevention of dental caries, *J. Evid. Base Dent. Pract.*, 2014, **14**, 95–102.
2 J. M. ten Cate and M. A. R. Buzalaf, Fluoride mode of action: Once there was an observant dentist, *J. Dent. Res.*, 2019, **98**, 725–730.
3 D. L. Ozsvath, Fluoride and environmental health: A review, *Rev. Environ. Sci. Biotechnol.*, 2009, **8**, 59–79.
4 W.-Z. Gai and Z.-Y. Deng, A comprehensive review of adsorbents for fluoride removal from water: Performance, water quality assessment and mechanism, *Environ. Sci.: Water Res. Technol.*, 2021, **7**, 1362–1386.
5 S. Jagtap, M. K. Yenkie, N. Labhsetwar and S. Rayalu, Fluoride in drinking water and defluoridation of water, *Chem. Rev.*, 2012, **112**, 2454–2466.
6 G. Singh, B. Kumari, G. Sinam, Kriti, N. Kumar and S. Mallick, Fluoride distribution and contamination in the water, soil and plants continuum and its remedial technologies, an Indian perspective-A review, *Environ. Pollut.*, 2018, **239**, 95–108.
7 J. Fawell, K. Bailey, J. Chilton, E. Dahi, L. Fewtrell and Y. Magara, *Fluoride in drinking-water*, Background Document for Development of WHO Guidelines for Drinking Water Quality, World Health Organization, IWA publishing, 2016.
8 M. Kleerekoper, The role of fluoride in the prevention of osteoporosis, *Endocrinol Metab. Clin. N. Am.*, 1998, **27**, 441–452.
9 S. Erdal and S. N. Buchanan, A quantitative look at fluorosis, fluoride exposure, and intake in children using a health risk assessment approach, *Environ. Health Perspect.*, 2005, **113**, 111–117.
10 W. Wei, S. Pang and D. Sun, The pathogenesis of endemic fluorosis: Research progress in the last 5 years, *J. Cell. Mol. Med.*, 2019, **23**, 2333–2342.
11 A. J. Malina, C. Lesseura, S. A. Busganga, P. Curtina, R. O. Wright and A. P. Sanders, Fluoride exposure and kidney and liver function among adolescents in the United States: NHANES, 2013–2016, *Environ. Int.*, 2019, **132**, 105012.
12 S. J. Wimalawansa, Molecular and cellular toxicity of fluoride in mystery, tubulointerstitial chronic kidney disease: A systematic review, *Rev. Environ. Sci. Biotechnol.*, 2020, **19**, 117–147.
13 P. P. Singh, M. K. Barjatiya, S. Dhing, R. Bhatnagar, S. Kothari and V. Dhar, Evidence suggesting that high intake of fluoride provokes nephrolithiasis in tribal populations, *Urol. Res.*, 2001, **29**, 238–244.
14 R. Siener and A. Hesse, Fluid intake and epidemiology of urolithiasis, *Eur. J. Clin. Nutr.*, 2003, **57**, S47–S51.
15 H. Guo, P. Kuang, Q. Luo, H. Cui, H. Deng, H. Liu, Y. Lu, J. Fang, Z. Zuo, J. Deng, Y. Li, X. Wang and L. Zhao, Effects of sodium fluoride on blood cellular and humoral immunity in mice, *Oncotarget*, 2017, **8**, 85504–85515.
16 S. Guth, S. Hüser, A. Roth, G. Degen, P. Diel, K. Edlund, G. Eisenbrand, K.-H. Engel, B. Epe, T. Grune, V. Heinz, T. Henle, H.-U. Humpf, H. Jäger, H.-G. Joost, S.-E. Kulling, A. Lampen, A. Mally, R. Marchan, D. Marko, E. Mühle, M. A. Nitsche, E. Röhrdanz, R. Stadler, C. V. Thriel, S. Vieths, R. F. Vogel, E. Wascher, C. Watzl, U. Nöthlings and J. G. Hengstler, Toxicity of fluoride: Critical evaluation of evidence for human developmental neuro-toxicity in epidemiological studies, animal experiments and in vitro analyses, *Arch. Toxicol.*, 2020, **94**, 1375–1415.
17 USEPA, *National primary drinking water regulations*, **https://www.epa.gov/ground-water-and-drinking-water/national-primary-drinking-water-regulations**.
18 A. Dhillon, M. Nair and D. Kumar, Analytical methods for determination and sensing of fluoride in biotic and abiotic sources: A review, *Anal. Methods*, 2016, **8**, 5338–5352.
19 P. Marocco, K. Sundseth, T. Aarhaug, A. Lanzini, M. Santarelli, A. O. Barnett and M. Thomassen, Online measurements of fluoride ions in proton exchange membrane water electrolysis through ion chromatography, *J. Power Sources*, 2021, **483**, 229179.
20 J. Musijowski, B. Szostek, M. Koc and M. Trojanowicz, Determination of fluoride as fluorosilane derivative using

reversed-phase HPLC with UV detection for determination of total organic fluorine, *J. Sep. Sci.*, 2010, **33**, 2636–2644.

21 Z. Qin, D. McNee, H. Gleisner, A. Raab, K. Kyeremeh, M. Jaspars, E. Krupp, H. Deng and J. Feldmann, Fluorine speciation analysis using reverse phase liquid chromatography coupled off-line to continuum source molecular absorption spectrometry (CS-MAS): Identification and quantification of novel fluorinated organic compounds in environmental and biological samples, *Anal. Chem.*, 2012, **84**, 6213–6219.

22 A. Akhdhar, M. Schneider, A. Orme, L. Schultes, A. Raab, E. M. Krupp, J. P. Benskin, B. Welz and J. Feldmann, The use of high 1resolution graphite furnace molecular absorption spectrometry (HR-MAS) for total fluorine determination in extractable organofluorines (EOF), *Talanta*, 2020, **209**, 120466.

23 A. Mallick, U. K. Roy, B. Haldar and S. Pratihar, A newly developed highly selective ratiometric fluoride ion sensor: Spectroscopic, NMR and density functional studies, *Analyst*, 2012, **137**, 1247–1251.

24 A. Tarai, Y. Li, B. Liu, D. Zhang, J. Li, W. Yan, J. Zhang, J. Qu and Z. Yang, A review on recognition of tri-/tetra-analyte by using simple organic colorimetric and fluorometric probes, *Coord. Chem. Rev.*, 2021, **445**, 214070.

25 Z. Li, J. R. Askim and K. S. Suslick, The optoelectronic nose: Colorimetric and fluorometric sensor arrays, *Chem. Rev.*, 2019, **119**, 231–292.

26 S. Dhiman, M. Ahmad, N. Singla, G. Kumar, P. Singh, V. Luxami, N. Kaur and S. Kumar, Chemodosimeters for optical detection of fluoride anion, *Coord. Chem. Rev.*, 2020, **405**, 213138.

27 J. Han, J. Zhang, M. Gao, H. Hao and X. Xu, Recent advances in chromo-fluorogenic probes for fluoride detection, *Dyes Pigm.*, 2019, **162**, 412–439.

28 S. Xiong, M. V. N. Kishore, W. Zhou and Q. He, Recent advances in selective recognition of fluoride with macrocyclic receptors, *Coord. Chem. Rev.*, 2022, **461**, 214480.

29 B. R. Jali, A. K. Barick, P. Mohapatra and S. K. Sahoo, A comprehensive review on quinones based fluoride selective colorimetric and fluorescence chemosensors, *J. Fluorine Chem.*, 2021, **244**, 109744.

30 L. Xu and J. Zhao, Bromine atom introduction improves the $F^-$ sensing ability of an indolo[3,2-b]carbazole-salicylaldehyde-based fluorescence turn-on sensor, *Chem. Commun.*, 2024, **60**, 3830–3833.

31 Q. Shen, S. Wang, N.-D. Yang, C. Zhang, Q. Wu and C. Yu, Recent development of small-molecule organic fluorophores for multifunctional bioimaging in the second near-infrared window, *J. Lumin.*, 2020, **225**, 117338.

32 Y. Liu, L. Wang, L. Xu and Y. Song, From aggregation-caused quenching to aggregation-induced delayed fluorescence: The impact of the effect of substituents, *J. Mater. Chem. C*, 2023, **11**, 13403–13417.

33 Y. Tang and B. Z. Tang, *Handbook of Aggregation-Induced Emission*, John Wiley & Sons Ltd, 2022.

34 Z. He, C. Ke and B. Z. Tang, Journey of aggregation-induced emission research, *ACS Omega*, 2018, **3**, 3267–3277.

35 P.-Y. Fu, S.-Z. Yi, M. Pan and C.-Y. Su, Excited-state intramolecular proton transfer (ESIPT) based metal–organic supramolecular optical materials: Energy transfer mechanism and luminescence regulation strategy, *Acc. Mater. Res.*, 2023, **4**, 939–952.

36 A. A. Bhosle, M. Banerjee, S. D. Hiremath, A. C. Bhasikuttan and A. Chatterjee, A new series of $D_1$-A-$D_2$-type ESIPT-TICT-AIE active orange-to-red emissive unsymmetrical azines: Their all-throughout mechanochemical synthesis and exploration of photophysical properties, *Chem.–Asian J.*, 2023, **18**, e202300048.

37 C. Li and J. Zhao, Organoplatinum complex exhibiting aggregation-enhanced emission (AEE) and dual-channel ion-sensing properties by terminating the molecular configuration transformation (MCT) and excited-state intramolecular proton transfer (ESIPT), *Inorg. Chem.*, 2024, **63**, 11757–11767.

38 A. A. Bhosle, S. D. Hiremath, A. C. Bhasikuttan, M. Banerjee and A. Chatterjee, Solvent-free mechanochemical synthesis of a novel benzothiazole-azine based ESIPT-coupled orange AIEgen for the selective recognition of $Cu^{2+}$ ions in solution and solid phase, *J. Photochem. Photobiol., A*, 2021, **413**, 113265.

39 I. Kaur, Shivani, P. Kaur and K. Singh, 2-(2′-Hydroxyphenyl) benzothiazole derivatives: Emission and color tuning, *Dyes Pigm.*, 2020, **176**, 108198.

40 Z.-J. Li, W.-J. Zhang, W.-Z. Bi, Q.-J. Ma, S.-X. Feng, X.-L. Chen and L.-B. Qu, An amino-substituted 2-(2′-hydroxyphenyl) benzimidazole for the fluorescent detection of phosgene based on an ESIPT mechanism, *RSC Adv.*, 2021, **11**, 10836–10841.

41 M. L. Odyniec, S.-J. Park, J. E. Gardiner, E. C. Webb, A. C. Sedgwick, J. Yoon, S. D. Bull, H. M. Kim and T. D. James, A fluorescent ESIPT-based benzimidazole platform for the ratiometric two-photon imaging of $ONOO^-$ in vitro and ex vivo, *Chem. Sci.*, 2020, **11**, 7329–7334.

42 T. Stoerkler, T. Pariat, A. D. Laurent, D. Jacquemin, G. Ulrich and J. Massue, Sterically hindered 2-(2′-hydroxyphenyl) benzoxazole (HBO) emitters: Synthesis, spectroscopic studies, and theoretical calculations, *Eur. J. Org Chem.*, 2022, **2022**, e202200661.

43 J. Massue, D. Frath, G. Ulrich, P. Retailleau and R. Ziessel, Synthesis of luminescent 2-(2′-hydroxyphenyl)benzoxazole (HBO) borate complexes, *Org. Lett.*, 2012, **14**, 230–233.

44 K. Pericherla, P. Kaswan, K. Pandey and A. Kumar, Recent developments in the synthesis of imidazo[1,2-a]pyridines, *Synthesis*, 2015, **47**, 887–912.

45 A. K. Bagdi, S. Santra, K. Monir and A. Hajra, Synthesis of imidazo[1,2-a]pyridines: A decade update, *Chem. Commun.*, 2015, **51**, 1555–1575.

46 G. C. Moraski, L. D. Markley, P. A. Hipskind, H. Boshoff, S. Cho, S. G. Franzblau and M. J. Miller, Advent of imidazo [1,2-a]pyridine-3-carboxamides with potent multi- and extended drug resistant antituberculosis activity, *ACS Med. Chem. Lett.*, 2011, **2**, 466–470.

47 S. Samanta, S. Kumar, E. K. Aratikatla, S. R. Ghorpade and V. Singh, Recent developments of imidazo[1,2-a]pyridine

analogues as antituberculosis agents, *RSC Med. Chem.*, 2023, **14**, 644–657.

48 M. Zhu, L. Wang, X. Wu, R. Na, Y. Wang, Q. X. Li and B. D. Hammock, A novel and simple imidazo[1,2-a]pyridin fluorescent probe for the sensitive and selective imaging of cysteine in living cells and zebrafish, *Anal. Chim. Acta*, 2019, **1058**, 155–165.

49 S. Debnath, S. Parveen, P. Pradhan, I. Das and T. Das, Benzo [4,5]imidazo[1,2-a]pyridines and benzo[4,5]imidazo[1,2-a] pyrimidines: Recent advancements in synthesis of two diversely important heterocyclic motifs and their derivatives, *New J. Chem.*, 2022, **46**, 10504–10534.

50 A. J. Stasyuk, M. Banasiewicz, M. K. Cyrański and D. T. Gryko, Imidazo[1,2-a]pyridines susceptible to excited state intramolecular proton transfer: One-pot synthesis via an Ortoleva–King reaction, *J. Org. Chem.*, 2012, **77**, 5552–5558.

51 T. Mutai, H. Sawatani, T. Shida, H. Shono and K. Araki, Tuning of excited-state intramolecular proton transfer (ESIPT) fluorescence of imidazo[1,2-a]pyridine in rigid matrices by substitution effect, *J. Org. Chem.*, 2013, **78**, 2482–2489.

52 L. Tong, Y. Yang, L. Zhang, J. Tao, B. Sun, C. Song, M. Qi, F. Yang, M. Zhao, J. Jiang and J. Design, synthesis of hydrogen peroxide response AIE fluorescence probes based on imidazo [1,2-a] pyridine, *Molecules*, 2024, **29**, 882.

53 M. Zhu, L. Wang, X. Wu, R. Na, Y. Wang, Q. X. Li and B. D. Hammock, A novel and simple imidazo[1,2-a] pyridine fluorescent probe for the sensitive and selective imaging of cysteine in living cells and zebrafish, *Anal. Chim. Acta*, 2019, **1058**, 155–165.

54 A. A. Bhosle, M. Banerjee, N. Barooah, A. C. Bhasikuttan, K. Kadu, S. R. Ramanan and A. Chatterjee, ESIPT-active hydroxybenzothiazole-picolinium@CB[7]-HAp NPs based supramolecular sensing assembly for spermine, spermidine and cadaverine: Application in monitoring cancer biomarkers and food spoilage, *J. Photochem. Photobiol., A*, 2022, **426**, 113770.

55 M. Banerjee, A. A. Bhosle, A. Chatterjee and S. Saha, Mechanochemical synthesis of organic dyes and fluorophores, *J. Org. Chem.*, 2021, **86**, 13911–13923.

56 D. Ozer, Mechanochemistry: A power tool for green synthesis, in *Advances in Green Synthesis: Avenues and Sustainability*, ed. Inamuddin, R. Boddula, M. I. Ahamed and A. Khan, Springer International Publishing, Cham, 2021, pp. 23–39.

57 T. Mutai, H. Sawatani, T. Shida, H. Shono and K. Araki, Tuning of excited-state intramolecular proton transfer (ESIPT) fluorescence of imidazo[1,2-a]pyridine in rigid matrices by substitution effect, *J. Org. Chem.*, 2013, **78**, 2482–2489.

58 R. R. Parr and R. G. Yang, *Density Functional Theory of Atoms and Molecules*, Oxford University Press, New York, 1989.

59 C. Jamorski, M. E. Casida and D. R. Salahub, Dynamic polarizabilities and excitation spectra from a molecular implementation of time-dependent density-functional response theory: $N_2$ as a case study, *J. Phys. Chem.*, 1996, **104**, 5134–5147.

60 R. Bauerschmitt and R. Alrichs, Treatment of electronic excitations within the adiabatic approximation of time dependent density functional theory, *Chem. Phys. Lett.*, 1996, **256**, 454–464.

61 R. Bauerschmitt, M. Häser, O. Treutler and R. Alrichs, Calculation of excitation energies within time-dependent density functional theory using auxiliary basis set expansions, *Chem. Phys. Lett.*, 1997, **264**, 573–578.

62 M. J. Frisch, G. W. Trucks, H. B. Schlegel, G. E. Scuseria, M. A. Robb, J. R. Cheeseman, J. A. Montgomery Jr, T. Vreven, K. N. Kudin, J. C. Burant, J. M. Millam, S. S. Iyengar, J. Tomasi, V. Barone, B. Mennucci, M. Cossi, G. Scalmani, N. Rega, G. A. Petersson, H. Nakatsuji, M. Hada, M. Ehara, K. Toyota, R. Fukuda, J. Hasegawa, M. Ishida, T. Nakajima, Y. Honda, O. Kitao, H. Nakai, M. Klene, X. Li, J. E. Knox, H. P. Hratchian, J. B. Cross, V. Bakken, C. Adamo, J. Jaramillo, R. Gomperts, R. E. Stratmann, O. Yazyev, A. J. Austin, R. Cammi, C. Pomelli, J. W. Ochterski, P. Y. Ayala, K. Morokuma, G. A. Voth, P. Salvador, J. J. Dannenberg, V. G. Zakrzewski, S. Dapprich, A. D. Daniels, M. C. Strain, O. Farkas, D. K. Malick, A. D. Rabuck, K. Raghavachari, J. B. Foresman, J. V. Ortiz, Q. Cui, A. G. Baboul, S. Clifford, J. Cioslowski, B. B. Stefanov, G. Liu, A. Liashenko, P. Piskorz, I. Komaromi, R. L. Martin, D. J. Fox, T. Keith, M. A. Al-Laham, C. Y. Peng, A. Nanayakkara, M. Challacombe, P. M. W. Gill, B. Johnson, W. Chen, M. W. Wong, C. Gonzalez and J. A. Pople, *Gaussian 03, Revision E.01*, Gaussian, Inc., Wallingford, CT, 2004.

63 D. Das, Z. T. Bhutia, P. C. Panjikar, A. Chatterjee and M. Banerjee, A simple and efficient route to 2-arylimidazo [1,2-a]pyridines and zolimidine using automated grindstone chemistry, *J. Heterocycl. Chem.*, 2020, **57**, 4099–4107.

64 Z. T. Bhutia, D. Das, A. Chatterjee and M. Banerjee, Efficient and "green" synthetic route to imidazo[1,2-a]pyridine by Cu(II)–ascorbate-catalyzed $A^3$-coupling in aqueous micellar media, *ACS Omega*, 2019, **4**, 4481–4490.

65 A. M. Brouwer, Standards for photoluminescence quantum yield measurements in solution (IUPAC Technical Report), *Pure Appl. Chem.*, 2011, **83**, 2213–2228.